Title: Nanoscale 'earthquake' effect induced by thin film surface acoustic waves as a new strategy for ice protection

Deyu Yang, Ran Tao, Xianghui Hou, Hamdi Torun, Glen McHale, James Martin, YongQing Fu**

D. Yang, Dr. Xianghui Hou
Faculty of Engineering, University of Nottingham, Nottingham, NG7 2RD, UK
E-mail: xianghui.hou@nottingham.ac.uk

Dr. R. Tao
Shenzhen Key Laboratory of Advanced Thin Films and Applications, College of Physics and Optoelectronic Engineering, Shenzhen University, Shenzhen, 518060, China

Dr. R. Tao, Dr. H. Torun, Prof. G. McHale, Prof. J. Martin, Prof. Y.Q Fu
Faculty of Engineering and Environment, Northumbria University, Newcastle upon Tyne, NE1 8ST, UK
E-mail: richard.fu@northumbria.ac.uk

Prof. G. McHale
School of Engineering, University of Edinburgh, Edinburgh EH9 3FB, UK

Keywords: Surface acoustic wave, icing, ice protection, icing monitoring

Abstract: Ice accretion often poses serious operational and safety challenges in a wide range of industries, such as aircraft, wind turbines, power transmission cables, oil field exploration and production and marine transport. Great efforts have been expended to research and develop viable solutions for ice prevention. Effective ice protection techniques, however, have yet to be developed. Ice prevention measures that are currently available often consume significant amounts of de-icing chemicals or energy, and these approaches are expensive to operate and have long-term economic and environmental impacts. In this study, a new ice protective strategy based on thin film surface acoustic waves (SAWs) is proposed that generates: nanoscale 'earthquake'-like vibrations, acoustic streaming, and acousto-heating effects, directly at the ice-structure interface, which actively and effectively delays ice nucleation and weakens ice adhesion on the structure surface. Compared with the conventional electro-thermal de-icing method, the SAW approach demonstrates a much-improved energy efficiency for ice-removal. The potential for the dual capability of

autonomous ice monitoring and removing functions using the SAW generation elements as transducers has also been explored.

1. Introduction

Ice accretion (*via* super-cooled humid air, frost formation, frozen condensation, or freezing rain) often poses serious operational and safety challenges in aviation[1], power transmission lines[2], offshore platforms[3], and wind turbine energy sectors[4]. The requirements to alleviate the economic and safety risks due to ice accretion have been increasing and this has driven the research to develop sustainable solutions for ice protection. Available active ice protection methods deploy resistance heating, hot air, radiation, de-icing fluids, electro-impulsive/expulsive, or ultrasonic waves[5-8]. These solutions often require significant energy or chemical consumption and form complex systems with low efficiencies. Passive ice protection methods, usually based on icephobic surfaces and coatings, include super-hydrophobic surfaces, slippery liquid-infused porous surfaces, and elastic coatings[9]. These methods either minimize or delay ice accretion on structural surfaces or lower the ice adhesion strength to facilitate ice removal if ice accumulation occurs; but are often limited in effectiveness and durability [9].

In this paper, we propose a new ice prevention strategy using thin film surface acoustic waves. Thin film SAW devices can generate nanoscale ‘earthquakes’ *via* surface wave vibrations[10] that we investigate as a method for ice protection. In addition to inducing controllable vibrations, SAWs can be used for localized surface heating[11-13] at the structural surface and ice-structure interfaces for highly efficient de-icing and anti-icing. Surface acoustic waves (SAWs) have recently been extensively applied in wireless communications, acoustofluidics, sensors, micro heaters, and biology[10]. Multiple hybrid wave modes (combining Rayleigh, Lamb, and shear horizontal SAWs) with different vibration amplitudes and phases can be readily generated using thin film coated SAW devices[14]. In this work, we

have investigated different wave propagation modes that can be optimized for both icing and de-icing strategies. Thin film-based SAWs are different from the conventional SAWs generated on bulk piezoelectric materials in that they are manufactured by depositing a piezoelectric thin film onto a common substrate[10]. Thin film based SAWs enable the integration of multiple functions onto different substrates such as silicon, glass, metal film, and polymer with arbitrary geometries[15-17], making the technology very advantageous for ice protection applications as they have good structural integrity and system integration capabilities. The propagated waves can be coupled into the water droplets that lead to turbulence and significant streaming, thus preventing ice nucleation. SAW devices can be operated wirelessly and can be used to monitor the icing process, which collectively enables automated and remote device operation for precise, on-demand de-icing applications.

2. Theory

2.1. Mechanisms of anti-icing and de-icing principle using thin film SAW

Thin film SAW devices used in this study were fabricated using piezoelectric ZnO thin films with nano-scale surface roughness, deposited on the industrial components such as Al substrates, which have a microscale roughness. A hydrophobic layer was further coated onto the ZnO film to enhance the hydrophobicity of the working surface, as illustrated in Figures 1(a) and 1(b) (in a 3D view with different dimension scales). At a given freezing temperature, when a water droplet is positioned on the ZnO thin film/Al surface, the surface hydrophobicity could offer a hybrid state of Wenzel and Cassie-Baxter states[18, 19], as illustrated in Figure 1(b). Ice nucleation and growth will happen when a thermodynamic equilibrium is reached at the water/structure interface, although the icephobic coating with the nano-micro-structured ZnO/Al surface could potentially delay the ice formation[20, 21]. According to classic nucleation theory, ice nucleation and growth can happen on an intrinsic rough surface as the nucleolus sites under a thermodynamic equilibrium condition. The

critical nucleolus radius, r_c, and the heterogeneous ice nucleation critical free energy, ΔG^*, at a given temperature T, can be written as[22]:

$$r_c = \frac{2\gamma_{IW}}{\Delta G_v} \quad (1)$$

$$\Delta G^* = \frac{16\pi\gamma_{IW}^3}{3\Delta G_V^2} f(m,x) \quad (2)$$

where $\Delta G_v = \Delta H_v \frac{(T_m - T)}{T_m}$ is the volumetric free energy of phase-change, ΔH_v is the enthalpy of phase-change, and T_m is the phase-transition temperature. $\gamma_{IW} = 23.24\left[\frac{T}{235.8}\right]^{0.35}$ is the interfacial tension of the water-ice nucleolus[22], $f(m,x)$ is a surface factor which is governed by the energy and geometry of the involved interfaces and defined as[22]:

$$f(m,x) = 1 + \left(\frac{1-mx}{g_v}\right)^3 + x^3\left[2 - 3\left(\frac{x-m}{g_v}\right) + \left(\frac{x-m}{g_v}\right)^3\right] + 3mx^2\left(\frac{x-m}{g_v} - 1\right) \quad (3)$$

$$g_v = (1 + x^2 - 2mx)^{\frac{1}{2}} \quad (4)$$

where the value of m depends on the surface energy of the interfaces (i.e., $m = \cos\theta = \frac{\gamma_{SW} - \gamma_{SI}}{\gamma_{WI}}$). γ_{SW}, γ_{SI}, and γ_{WI} denotes the surface energy values of solid-water, solid-ice, and water-ice interface, respectively. The value of x $(= \frac{R}{r_c})$ depends on the radius of features at the surface (R) and the critical nucleolus radius (r_c). Another key factor to evaluate the ice formation is the nucleation rate, $J(T)$, which is given by[23]:

$$J(T) = \tau^{-1} = K\ exp\left(-\frac{\Delta G^*}{k_B T}\right) \quad (5)$$

where τ is the ice nucleation delay time, k_B is the Boltzmann constant, $K(= Z\beta N)$ is a kinetic constant which depends on the Zeldovich non-equilibrium factor (Z), the rate at which atoms or molecules are added to the critical nucleus (β), and the number of atomic nucleation sites per unit volume (N). According to equations (1), (2), and (5), the key factors of ice nucleation on the given structural surface are the temperature T and the surface factor $f(m,x)$.

2.2. Anti-icing principle using thin film SAW

When the SAW is generated and propagates along the surface as shown in Figures 1(c) and 1(d), the nanoscale 'earthquake' effect, acoustic radiation force[24], acoustic streaming[25, 26], and acoustic thermal effect (which is often called acousto-thermal effect)[27] will all influence ice nucleation and growth.

One of the main adhesive forces between the ice nucleolus and the solid surface is *Van der Waal*'s force, whose bond length is 0.4-0.5 nm and bond energy is 2-15 kJ/mol[28]. Once the ice nucleolus is formed, the nanoscale 'earthquake' effects on the device surface induced by SAW cause significant surface vibrations and thus decrease the adhesion of the ice nucleolus formed on the surface. Simultaneously, the acousto-thermal effect (SAW radiation and energy dissipation as well as the associated Joule thermal effect) introduces localized thermal energy at the ice/structure interface which leads to the increase of temperatures of solid surface and surrounding liquid [13, 29-31] as illustrated by the thermal gradient shown in Figure 1(d). According to equations (2) to (5), the increasing temperature (T) at the ice-structure interface will increase the ice nucleation critical free energy ΔG^* and decrease the ice nucleation rate $J(T)$, which means that the ice nucleation is restricted. Therefore, this acousto-thermal effect will restrain the growth of the ice nucleus and also weaken its interfacial bonds to the solid surface.

According to acoustofluidic theories, when the SAW energy is dissipated into the liquid, there are two different types of forces acted onto solid particles (ice nucleus in this case) suspended in the liquid, i.e., acoustic radiation force (F_R) and acoustic streaming drag force (F_d)[10]. A dimensionless coefficient (κ) was introduced to evaluate which force is dominant in different liquids with various particles, and this can be written as[32]:

$$\kappa = \frac{2\pi r}{\lambda} \qquad (6)$$

where λ is the wavelength of the acoustic wave in a liquid medium and r is the radius of the solid particles. If κ≥1, a net acoustic radiation force drives the movement of particles in the

fluid flow. If κ<1, the acoustic streaming is dominant in the system, and the suspended particles follow the streaming flows. According to Equation (1), the critical nucleolus radius at -10 ℃ is ~4.74 nm, based on literature [23]. With the wavelength of SAW devices varying from 100 μm to 400 μm in this study, the values of κ change from 7.44×10^{-5} to 29.8×10^{-5}, which are far less than 1. This indicates that the ice nucleolus inside the liquid is mainly driven by acoustic streaming.

When the SAW is applied and propagated into the liquid, the accompanied microstreaming or flow will lead to the relative motion between the ice nucleolus and liquid medium. This flow increases with the increase of SAW's wavelength and applied power[10, 33]. Based on the above discussion, the formed ice nucleoli, which are easily detached from the surface into the liquid due to the nanoscale vibrations and acousto-thermal effect, will easily flow along with the acoustic streaming of the liquid. This flow will restrict the rapid growth of ice nucleoli, thus enhancing the anti-icing performance.

2.3. De-icing principle using thin film SAW

Energy efficiency is the key factor to be considered when evaluating the effectiveness of SAWs for de-icing. Figures 1(e) and 1(f) illustrate the ice-structure interface. According to reference[34], there are four types of interfacial forces applied at the ice-solid interface: *Van der Waals* force, electrostatic force, hydrogen bonding, and mechanical adhesion. Firstly, the nanoscale vibration introduced by SAWs has a similar scale with the bond length of *Van der Waals* force, and thus leads to the weakening of ice bonds. Tiny cracks (or air voids) are often formed at the ice-structure interface during the icing process, and the nanoscale 'earthquakes' generated by the SAWs can effectively enhance the rapid growth of these cracks. Additional new cracks can also be generated due to the significant vibrations at the interface. The formation and propagation of these cracks reduce the mechanical adhesion of ice to the solid surface as illustrated in Figure 1(f). Furthermore, the acousto-thermal effect leads to the local

melting of the interfacial ice layer and significantly minimizes the ice adhesion force, which results in an efficient de-icing process (see Figure 1(f)).

3. Results and discussion

3.1. Anti-icing with water droplets on SAWs

Three different icing phenomena of water droplets were observed in all the anti-icing experiments, as shown in Figure 2. In the first case (the first row in Figure 2), the droplet was kept clear and transparent during the whole icing process when there was no SAW power applied to the device. Icing started at the water/structure interface, where a dynamic interface of ice growth was observed at the bottom of the droplet close to the device surface. As the icing proceeded, the ice/water interface gradually rose from the bottom to the top of the droplet. The whole icing process was ended when a sharp tip was formed at the top of the droplet. For this kind of transparent icing phenomenon without SAW power applied, the icing time was ~50s ± 4s.

Similar to those without any power applied, for the devices with 100 μm wavelength and the resonant frequency of 27.84 MHz (applied power of 0.07 W and 0.15 W) and 200 μm wavelength and the resonant frequency of 14.32 MHz (applied power of 0.07 W), the icing process of droplets still showed a transparent feature (slightly translucent). Whereas the icing time was delayed according to the applied power, for example, from 50s ± 4s without any power to 78s ± 5s at a power of 0.07 W for 100 μm wavelength devices.

For the SAW devices with a larger wavelength and/or applied with higher SAW power (e.g., 100 μm with 0.25 W; 200 μm with 0.15 W; and 300 μm with 0.07 W), a different icing phenomenon (often called supercooled icing phenomenon)[35, 36] appeared in the droplets as shown in the second row in Figure 2. For the device with 300 μm wavelength and 0.07 W power, the droplet was kept supercooled without any icing occurring during the initial stage. The whole droplet was vibrated slightly, and a streaming phenomenon was clearly observed

inside the liquid. After the process proceeded for ~46 s, the droplet was suddenly transformed from the transparent liquid into an opaque appearance. Simultaneously, a dynamic ice/liquid interface was appeared at the bottom and quickly rose upwards to the top of the droplet until the sharp tip was formed indicating the end of the icing process, which took ~95 s to complete. A recorded video of the supercooled icing process on the SAW device with the applied power of 0.07 W and the wavelength of 300 μm is attached in the supporting information.

The third row in Figure 2 shows another icing phenomenon. The droplet was kept in a supercooled liquid state with the SAW power applied during the whole 10-min experimental period without any icing phenomenon, and obvious vibration and streaming phenomena were observed inside the droplet. These were observed for the SAW devices with a wavelength of 400 μm and a power of 0.07 W; those with wavelengths of 300 μm and 400 μm and a power of 0.15 W; as well as those with wavelengths of 200 μm, 300 μm and 400 μm and a power of 0.25 W. We defined the icing time of this phenomenon as >600 s (e.g., >10 min), due to absence of icing up to the end of experiments.

Table 1 lists all the icing durations obtained at different applied powers and wavelengths, presenting a clear delayed trend of the ice nucleation process after the SAWs have been applied. In Table 1, the first type of icing phenomenon with the transparent features is shown in the orange area (e.g., the first row in Figure 2). The second type (e.g., the second row in Figure 2), supercooled icing phenomenon, is shown in those blue areas. The third type of icing phenomenon is shown in the green area (e.g., the third row in Figure 2) in which no icing was observed during the whole 10-minute experiment.

When there was no SAW power supplied, the ice-nucleation at the solid surface followed the classical ice-formation theory[22, 23]. Due to the same environmental conditions (e.g. same temperature) and similar surface structure (e.g., roughness), for all the devices, the critical nucleolus radius, the critical free energy of ice nucleation, and nucleation rate (according to

equations (1) to (5)) were maintained nearly as constants which led to similar icing times of around 50 s for all the devices without SAW power applied.

With the power applied and SAWs generated, as explained before, the nanoscale 'earthquake', acousto-thermal effect, and acoustic streaming delayed the ice nucleation, thus leading to the increase of icing time or the absence of icing. Firstly, for a device with a given wavelength, the icing was delayed with the increase of applied power. When a relatively low power of 0.07 W was applied to the SAW sample with a wavelength of 200 μm, the icing time was extended to 80 s ± 4 s. The ice was formed in a transparent mode, which was the same as that for the device without any SAW power applied. When the power was increased to 0.15 W, the icing process became supercooled mode with the icing time of 237 s ± 10 s. As the power was further increased to 0.25 W, no icing was observed in the droplet and the icing time was increased to >600 s. According to acoustic wave theories[10, 30, 32], with the increase of applied power, the intensity of surface vibration and the acousto-thermal effect are increased correspondingly which means more SAW energy is transferred into the liquid droplet with the SAW. The ice nucleation is significantly restrained, especially as the acousto-thermal heating effect becomes more significant at a higher SAW power. Meanwhile, the streaming or microflow inside the droplet is also enhanced with the increased SAW power[10, 18, 32]. The stronger acoustic streaming force also enhances the detachment of ice nucleolus from the surface of devices and leads to the delayed icing generation with the increase of power.

On the other hand, at a given power, the delay of icing became more obvious with the increase of wavelength. When the power was 0.15 W, for example, the icing process of the device with 100 μm wavelength remained in a transparent icing process in which the icing time was increased to 63 s ± 8 s. When the wavelength was increased to 200 μm, the icing process was transferred into a supercooled manner and the icing time was increased to 237 s

±10 s. As for the devices with wavelengths of 300 μm and 400 μm and at the same power of 0.15 W, no icing was observed, and the icing time was increased to the values greater than 600 s. The increased wavelength means higher amplitude of SAWs are generated, equivalent to stronger vibrations at ice nucleolus/structure interface, and also stronger streaming phenomena inside the droplets, both of which lead to the delayed icing trend.

According to the research of acousto-thermal effect[29], the increase of the SAW wavelength leads to a decrease in heating effect which is attributed to the reduction in acoustic energy density in the whole droplet. The possible reason is that with the increase of wavelength, the increased acoustic streaming and internal microflow enhance the convection inside the droplet which strengthens the transfer of liquid and heat[37]. This enhancement overcomes the weakening of the acousto-thermal effect and keeps the supercooled state of the surface droplets.

3.2. Ice block de-icing using SAW devices for low energy consumption

The de-icing experiments were performed by measuring and calculating overall energy consumption for the ice blocks to detach from device surface after the SAW has been applied. Figure 3 shows the results of de-icing energy density (energy consumption per unit area) of the devices using both the SAWs and conventional electro-thermal methods. Clearly, the consumed energy density was decreased significantly with the increase of wavelength from 100 μm to 300 μm until reaching a minimum at 300 μm for a given SAW power. As the wavelength was increased to 400 μm, energy consumption was increased slightly but was still much lower than the energy consumed using the conventional electro-thermal method. The energy consumption of the electro-thermal method was found to be greater than those for most of the SAW devices except that with a wavelength of 100 μm. The results prove that compared with the conventional electro-thermal de-icing method, applying SAWs into the de-icing process can achieve an ultra-high energy efficiency gain of approximately 7 times if the device wavelength is between 200 to 300 μm. A video showing the de-icing process using the

SAW device with a wavelength of 300 μm and an applied power of 4 W is attached in the Supporting Information.

In general, the surface nanoscale 'earthquake' and acousto-thermal heating effects are the two main reasons for the weakened binding force at the ice/structure interface. According to the literature [13, 31], the amplitudes of surface vibrations are directly proportional to both the applied power and the wavelength. The acousto-heating effect is inversely proportional to the frequency which means the smaller wavelength leading to a more significant heating effect. The de-icing process can be seen as the synergistic effect of the above two mechanisms. Firstly, when the wavelength was increased from 100 μm to 300 μm, the larger amplitude nanoscale 'earthquake' was dominant and thus more mechanical cracks were generated, which weakened the binding force at the ice/structure interface. When the wavelength was increased to 400 μm, surface vibration became much stronger, but the ratio of energy consumption on acousto-heating would be reduced , leading to the increase of average energy consumption.

Our results show that the SAW devices perform much more efficiently than the electro-thermal de-icing method except for the case when the wavelength is 100 μm. The electro-thermal method generally uses the Joule heating effect to weaken the ice/solid interface. Our results prove that when the SAW wavelength is relatively small (100 μm), the SAW induced acoustic vibration is not strong enough to break interfacial bonds effectively and the acoustic heating effect is not as effective as the Joule effect. However, with the increase of wavelength (200-400 μm), the synergistic effects of nanoscale vibration and acoustic heating made the SAW methods more effective and energy-efficient than the conventional electro-thermal method in the de-icing process.

3.3. Ice monitoring-removing autonomous system

Ice repellency in a humid environment and icing monitoring capability of SAW devices were further studied and the potential for ice monitoring-removing autonomous system wase

explored. For the SAW device with a constant wavelength in a humid environment, the applied SAW will delay the icing process, which became more significant with the increase of applied power. The ice accretion phenomena with various applied SAW powers in the 20-minute icing process are shown in Figure 4(a). Without any power applied, distinct ice accretion could be observed on the SAW devices. An apparent reduction of the icing was observed at the same stage with the 0.5 W power supplied. As the power was increased to 1.2 W, there was no obvious ice formed on the sample surface during the whole experimental process. Figure 4(b) shows the measured ice weights as a function of applied SAW power on the device with 300 μm wavelength. There is a regular reduction of ice accretion with the increase of applied power.

Figures 5(a) to 5(c) show the measured S11 reflection signal of the POTS coated SAW device (with a wavelength of 300 μm) with different powers of 0 W, 0.49 W, and 1.20 W during aerosol supplied icing process. When there was no SAW power applied, the resonant frequencies of S11 signals were decreased significantly and continuously with the increase of time as shown in Figure 5(a), which is mainly due to the built-up of the ice accretion. However, at the same conditions but applying a SAW power of 0.49 W on the SAW device, the shifts of resonant frequency (S11 signals) were dramatically decreased if compared with those without any SAW power applied as shown in Figure 5(b). The dramatic reduction of frequency shifts is mainly due to the gradual removal of the ice layer on the devices. When the applied power was increased to 1.20 W, the SAW signals of the SAW device have not shown obvious resonant frequency shifts during the whole experimental process (see Figure 5(c)), which is mainly due to the effective and fast ice removal due to the SAW power. Figure 5(d) summarizes the obtained resonant frequency shifts of the SAW device applied with various applied powers during the icing process. There was a regular trend that the measured resonant frequency shift was significantly reduced with the increasing SAW power.

The frequencies were shifted obviously with the icing process, as the ice accretion on the surface changes the mass loading and the conductivity of the SAW devices. It is worthwhile to point out that the frequency shifts of the device were decreased remarkably after the SAW power was applied to remove the ice, because of effective anti-icing and de-icing effects generated by the SAWs. Besides proving the good deicing capability of the SAW device, our results also demonstrate that SAW devices can be used as a sensitive icing monitoring device, based on the frequency shift of the SAW signals. The above results prove that SAW devices have the potential to integrate into an autonomous system that can monitor surface ice accretion, and if necessary, the SAW devices can be switched on to remove attached ice.

4. Conclusion

We introduced a new ice prevention strategy in this work based on SAWs that can be applied to effectively restrain the ice nucleation and weaken the ice adhesion at the ice-structure interface, effective for both anti-icing and de-icing applications. We demonstrated that icing nucleation of water droplets is delayed with the increase of SAW power and wavelength. Our experiments revealed the main mechanisms for the delayed icing are the generation of nanoscale ‘earthquake’, acoustic streaming force inside the droplet, and acousto-thermal effect. Compared with the conventional electro-thermal de-icing method, SAW devices showed a much higher energy efficiency for the ice-removal process. With the increase of SAW wavelength, the de-icing energy consumption was decreased, reaching a minimum at the wavelength of 300 μm. The energy consumption was increased slightly when the wavelength increased to 400 μm. The SAW devices also showed a good effect on ice repellency in the moist environment. The decreased resonant frequency shifts of the SAW devices were observed with the increase of power due to the effective anti-icing and de-icing effects. The sensitive monitoring of the resonant frequency shifts and their good ice

repellency proved SAW devices can be used to design an effective ice monitoring-removing autonomous system.

5. Experimental Section/Methods

5.1 Preparation of the devices

A ZnO film of ~5 μm thick was deposited on 1.5 mm-thick Al plates using the DC magnetic sputtering technique. A zinc target with 99.99% purity was used during the deposition. The DC power was 400 W and the Ar/O_2 gas flow was 10/15 (in the unit of sccm). The interdigital transducers (IDTs) were patterned on top of ZnO thin film through a conventional lift-off process. A bilayer of Cr/Au with a thickness of 20 nm/100 nm was prepared using a thermal evaporator (EDWARDS AUTO306) as the electrode. The IDTs were designed with wavelengths of 100 μm, 200 μm, 300 μm, and 400 μm, comprising 42, 62, 41, and 31 pairs of electrodes, respectively. The corresponding Rayleigh wave frequencies measured using the network analyzer were 27.84, 14.32, 9.72, and 7.38 MHz. The SAW devices were then placed in a sealed vessel with 300 μL of 1H,1H,2H,2H-perfluorooctyltriethoxysilane (POTS) at 180 ℃ for 3 hrs to achieve a monolayer coating of POTS[38]. SAWs with different resonant frequencies were generated using a signal generator (9 k-2.4 GHz 2024, Marconi Instruments) and a power amplifier (Model 75A250, Amplifier Research). The static water contact angles on the untreated ZnO surfaces and the POTS coated surfaces were measured using a contact angle goniometer (FTA200, First Ten Angstorms, Inc., Portsmouth, VA, USA) with pumping out rate of 2μL/s, and the results are shown in Fig. S1. The root mean square roughness of ZnO/Al surfaces was calculated from the surface morphology image obtained using an atomic force microscope (AFM, Veeco Dimension 3100), shown in the Supporting Information (Fig. S2).

5.2 Anti-icing experiments

All the anti/de-icing experiments were performed in a freezing chamber which was built based on a cold plate (Para Cooler A, Para Cooler O, Weinkauf Medizintechnik, Germany). A transparent resin shield was assembled to form an enclosed chamber with good thermal insulation. The temperature was controlled by the cold plate, and uniform temperature distribution was obtained by an electric fan in the chamber. Prior to the experiments, all samples were placed in the chamber for 30 minutes to achieve a thermal equilibrium condition. The SAW devices with wavelengths of 100 μm, 200 μm, 300 μm, and 400 μm were first placed in the chamber (where the temperature and humidity were set to be -10 ℃ and 20%, respectively) and agitated with the input powers of 0 W, 0.07 W, 0.15 W, and 0.25 W, respectively. Then a deionized water droplet with a volume of 60 μl was placed onto the surface using a pipette to form a hemispherical shape with a diameter of ~6.12 mm. A digital camera was used to monitor the icing process and icing time (τ). The recording time for each sample was 10 minutes.

5.3 De-icing experiments

The de-icing experiments were performed at -10 ℃ in the freezing chamber with a controlled humidity of 20%. A rubber mold was filled with deionized water (with a mass of ~2 g and an icing area of 169.56 mm^2) and then transferred onto the surface of SAW devices. All the samples were placed in the freezing chamber for 18 hrs to form identical glazed ice blocks on the surface. During de-icing testing, the samples were vertically positioned, and then their gravity caused the ice blocks to slide down during the SAW tests, once de-icing was initiated. The SAW devices with wavelengths of 100 μm, 200 μm, 300 μm, and 400μm were agitated with the applied powers of 2.4 W, 3.2 W, 3.6 W, and 4.0 W, respectively. The de-icing process was recorded to obtain the ice detachment time and the overall energy consumption was calculated accordingly. A conventional electro-thermal de-icing method was also performed with a one-dimensional multi-lamina heat conduction configuration for the same devices without any SAW applied[39]. The applied power for electro-thermal devices was 2.86

W (input voltage 22 V) during testing. Their energy requirements were calculated for comparison purposes.

5.4 Ice monitoring and prevention experiments

An atomizer was used to generate and input water aerosols into the freezing chamber to keep the environmental humidity over 89% and simulate the icing process in a misty environment. The temperature of the freezing chamber was maintained at -6.5 ℃. Meanwhile, the SAW devices with a wavelength of 300 μm were agitated with different input powers of 0.25 W, 0.49 W, 0.79 W, and 1.20 W to evaluate their anti-icing performance.

A high-speed camera (Phantom V2511, 300 FPS) was used to record the entire icing process (20 minutes). The mass of ice built-up on different samples was calculated by measuring the weights of SAW devices before and immediately after (less than 1 s) the icing process. During the experiments, the resonant frequency of the SAW signals was collected every 5 minutes using the network analyzer, in order to monitor the ice build-up. For all the tests, a control sample without any power applied was set and the obtained results were used to verify the performance of the anti-icing performance of the SAW devices.

Acknowledgments

Deyu Yang and Dr. Ran Tao contributed equally to this work.
This work was financially supported by the UK Engineering and Physical Sciences Research Council (EPSRC) grants EP/P018998/1, Special Interests Group of Acoustofluidics under the EPSRC-funded UK Fluidic Network (EP/N032861/1), and Natural Science Foundation of SZU (Grant no. 860/000002110816). We also would like to acknowledge the support from EPSRC Centre for Doctoral Training in Renewable Energy Northeast Universities (ReNU) for funding through grant EP/S023836/1, the Propulsion Futures Beacon project, the University of Nottingham, and the joint Ph.D. studentship between the China Scholarship Council (CSC) and the University of Nottingham.

Received: ((will be filled in by the editorial staff))
Revised: ((will be filled in by the editorial staff))
Published online: ((will be filled in by the editorial staff))

Conflict of Interest

There is no conflict of interest concerning the work described in this manuscript.

References

[1] Y. Cao, Z. Wu, Y. Su, Z. Xu, *Prog Aerosp Sci.* **2015,** *74*, 62-80.

[2] S. Wang, X. Jiang, *Front. Inf. Technol. Electron. Eng.* **2012**.

[3] C. C. Ryerson, *Cold Reg Sci Technol.* **2011,** *65* (1), 97-110.

[4] O. Parent, A. Ilinca, *Cold Reg Sci Technol.* **2011,** *65* (1), 88-96.

[5] O. Fakorede, Z. Feger, H. Ibrahim, A. Ilinca, J. Perron, C. Masson, *Renew Sust Energ Rev.* **2016,** *65*, 662-675.

[6] V. Daniliuk, Y. Xu, R. Liu, T. He, X. Wang, *Renew Energy.* **2020,** *145*, 2005-2018.

[7] N. Dalili, A. Edrisy, R. Carriveau, *Renew Sust Energ Rev.* **2009,** *13* (2), 428-438.

[8] Z. Wang, *Energy Build.* **2017,** *140*, 42-49.

[9] M. J. Kreder, J. Alvarenga, P. Kim, J. Aizenberg, *Nat Rev Mater.* **2016,** *1* (1), 1-15.

[10] Y. Q. Fu, J. Luo, N.-T. Nguyen, A. Walton, A. J. Flewitt, X.-T. Zu, Y. Li, G. McHale, A. Matthews, E. Iborra, *Prog Mater Sci.* **2017,** *89*, 31-91.

[11] W. Connacher, N. Zhang, A. Huang, J. Mei, S. Zhang, T. Gopesh, J. Friend, *Lab Chip.* **2018,** *18* (14), 1952-1996.

[12] R. Kryshtal, A. Kundin, A. Medved, V. Shemet, *Tech. Phys. Lett.* **2002,** *28* (1), 50-51.

[13] J. Kondoh, N. Shimizu, Y. Matsui, S. Shiokawa, *IEEE Trans Ultrason Ferroelectr Freq Control.* **2005,** *52* (10), 1881-3.

[14] R. Tao, J. Reboud, H. Torun, G. McHale, L. E. Dodd, Q. Wu, K. Tao, X. Yang, J. T. Luo, S. Todryk, *Lab Chip.* **2020,** *20* (5), 1002-1011.

[15] Y. Wang, X. Tao, R. Tao, J. Zhou, Q. Zhang, D. Chen, H. Jin, S. Dong, J. Xie, Y. Q. Fu, *Sens Actuators A Phys.* **2020**, 111967.

[16] Q. Zhang, Y. Wang, R. Tao, H. Torun, J. Xie, Y. Li, C. Fu, J. Luo, Q. Wu, W. P. Ng, *J Micromech Microeng.* **2020**.

[17] J. Li, S. H. Biroun, R. Tao, Y. Wang, H. Torun, N. Xu, M. Rahmati, Y. Li, D. Gibson, C. Fu, *J Phys D Appl Phys.* **2020**.

[18] R. Tao, G. McHale, J. Reboud, J. M. Cooper, H. Torun, J. Luo, J. Luo, X. Yang, J. Zhou, P. Canyelles-Pericas, Q. Wu, Y. Fu, *Nano Lett.* **2020,** *20* (5), 3263-3270.

[19] A. Sudeepthi, L. Yeo, A. J. A. P. L. Sen, **2020,** *116* (9), 093704.

[20] Q. Hao, Y. Pang, Y. Zhao, J. Zhang, J. Feng, S. Yao, *Langmuir.* **2014,** *30* (51), 15416-15422.

[21] H. Sojoudi, M. Wang, N. D. Boscher, G. H. McKinley, K. K. Gleason, *Soft Matter.* **2016,** *12* (7), 1938-63.

[22] N. H. Fletcher, *J Chem Phys.* **1958,** *29* (3), 572-576.

[23] P. Irajizad, S. Nazifi, H. Ghasemi, *Adv Colloid Interface Sci.* **2019,** *269*, 203-218.

[24] G. Destgeer, B. Ha, J. Park, H. J. Sung, *Anal Chem.* **2016,** *88* (7), 3976-81.

[25] M. Alghane, B. Chen, Y. Q. Fu, Y. Li, J. Luo, A. Walton, *J Micromech Microeng.* **2010,** *21* (1), 015005.

[26] M. Alghane, B. X. Chen, Y. Q. Fu, Y. Li, M. P. Desmulliez, M. I. Mohammed, A. J. Walton, *Phys Rev E.* **2012,** *86* (5 Pt 2), 056304.

[27] R. J. Shilton, V. Mattoli, M. Travagliati, M. Agostini, A. Desii, F. Beltram, M. Cecchini, *Adv Func Mater*. **2015,** *25* (37), 5895-5901.

[28] R. Chang, *Physical chemistry for the biosciences*. University Science Books: **2005**.

[29] P. K. Das, A. D. Snider, V. R. Bhethanabotla, *Phys Fluids.* **2019,** *31* (10), 106106.

[30] T. Zheng, C. Wang, Q. Hu, S. Wei, *Appl Phys Lett.* **2018,** *112* (23), 233702.

[31] K. J. Suthar, S. K. Sankaranarayanan, M. Richardson, V. R. Bhethanabotla In *Liquid heating can cause denaturation of sensing layer in SAW biosensors*, SENSORS, 2013 IEEE, IEEE: **2013**; pp 1-4.

[32] M. Wu, A. Ozcelik, J. Rufo, Z. Wang, R. Fang, T. Jun Huang, *Microsyst Nanoeng.* **2019,** *5*, 32.

[33] A. Sudeepthi, A. Sen, L. J. M. Yeo, Nanofluidics, **2019,** *23* (5), 76.

[34] I. A. Ryzhkin, V. F. Petrenko, *J Phys Chem B.* **1997,** *101* (32), 6267-6270.

[35] J. J. J. o. t. A. S. Hallett, **1964,** *21* (6), 671-682.

[36] T. Wang, Y. Lü, L. Ai, Y. Zhou, M. J. L. Chen, **2019,** *35* (15), 5162-5167.

[37] D. Beyssen, F. Sarry, T. J. P. e. Roux-Marchand, **2015,** *120*, 1067-1070.

[38] J. Liu, Z. A. Janjua, M. Roe, F. Xu, B. Turnbull, K. S. Choi, X. Hou, *Nanomaterials.* **2016,** *6* (12), 232.

[39] Y. Zheng, J. Wang, J. Liu, K.-S. Choi, X. Hou, *Thin Solid Films.* **2019,** *687*.

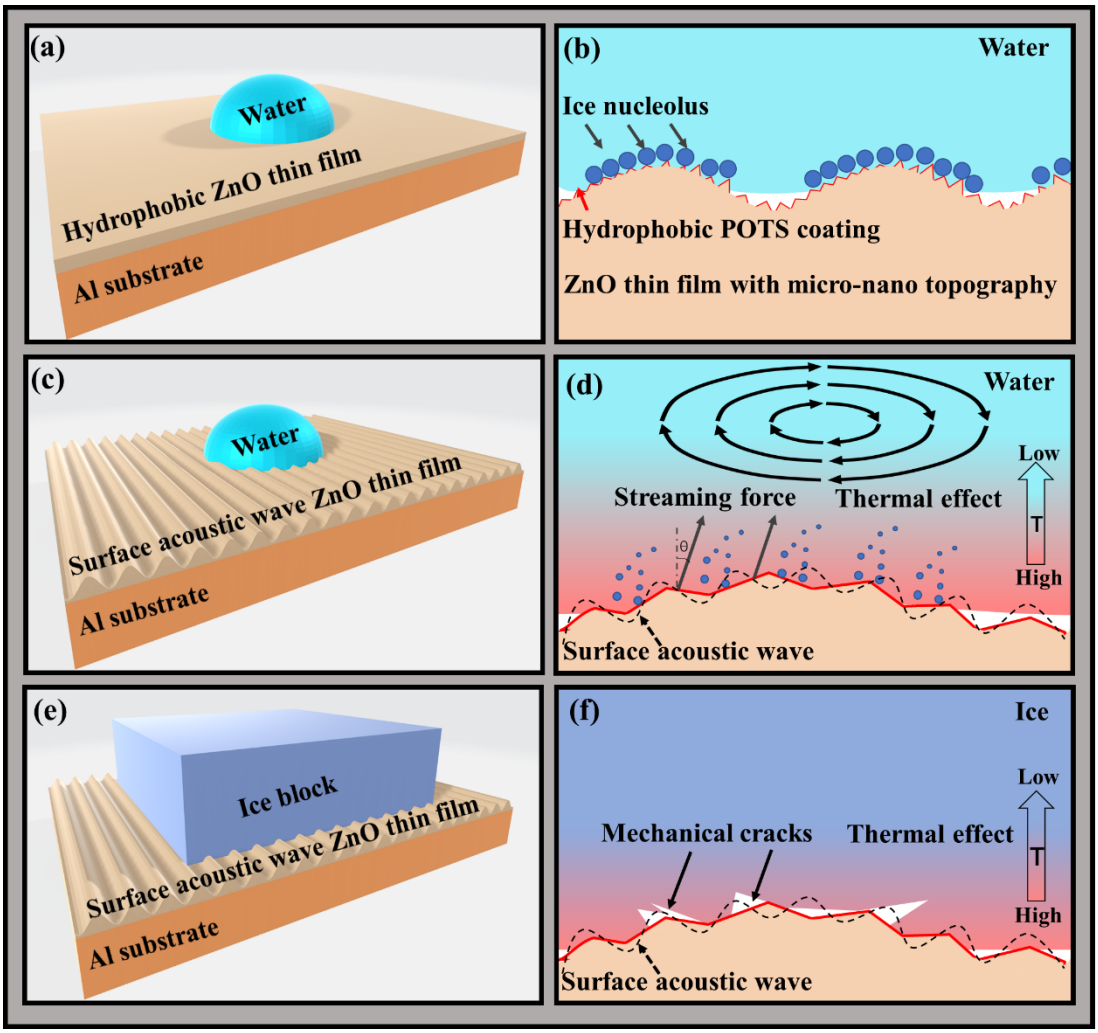

Figure 1. Schematic illustrations of the multi-layered integrated device: (a) a 3D model of hydrophobic SAW device without power applied; (b) a zoomed side-view of ice nucleation at the water-structure interface; (c) a 3D model of hydrophobic SAW device with power applied in anti-icing process; (d) a zoomed side-view of SAW anti-icing mechanism; (e) a 3D model of hydrophobic SAW device with power applied in the de-icing process; (f) a zoomed side-view of SAW de-icing mechanism.

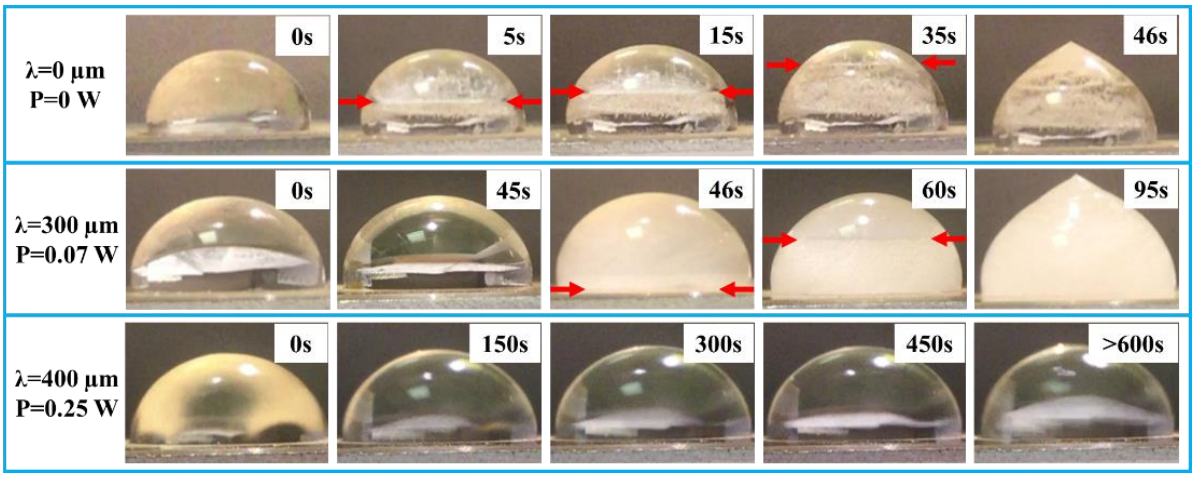

Figure 2. Droplet types of icing phenomena for SAW samples with different wavelengths and applied powers. (Droplet volume is 60 μl)

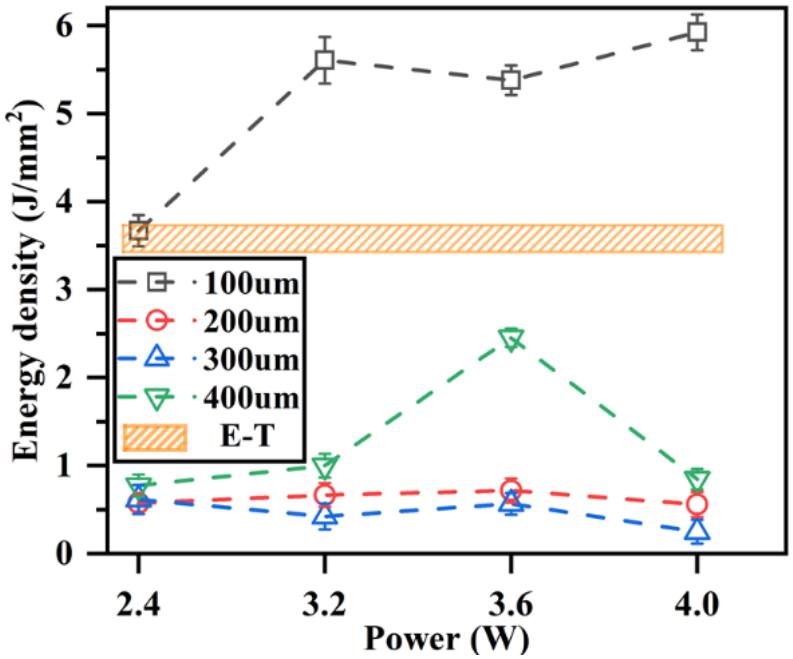

Figure 3. Energy consumption of SAW and the conventional electro-thermal (E-T) methods during the de-icing process.

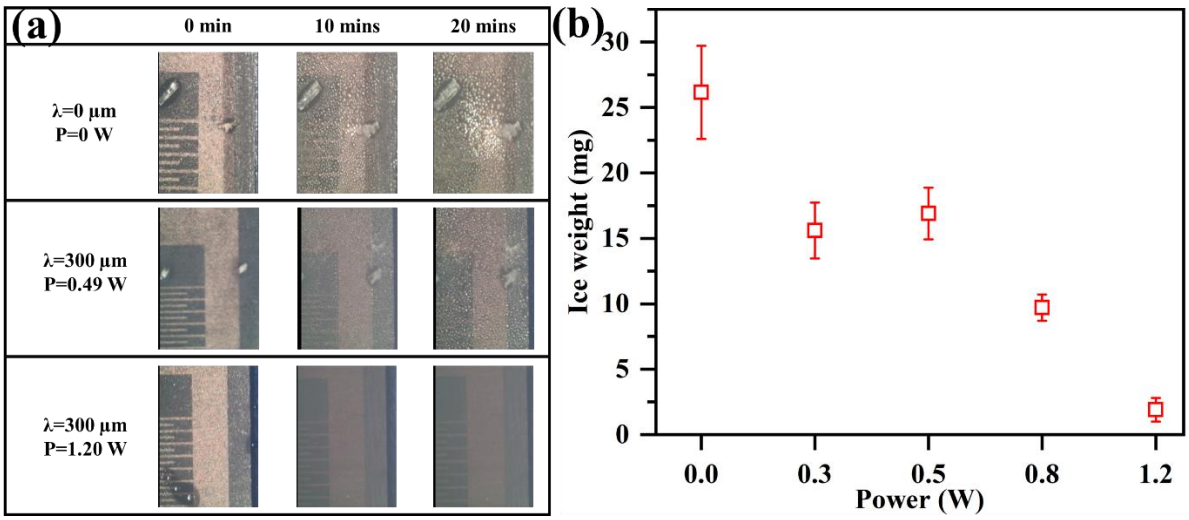

Figure 4. Icing results of POTS deposited 300 μm SAW device when various power supplied. (a) Icing process images of no power, 0.5 W and 1.2 W power supplied; (b) Ice weight measured at different SAW powers after 20-minute power duration.

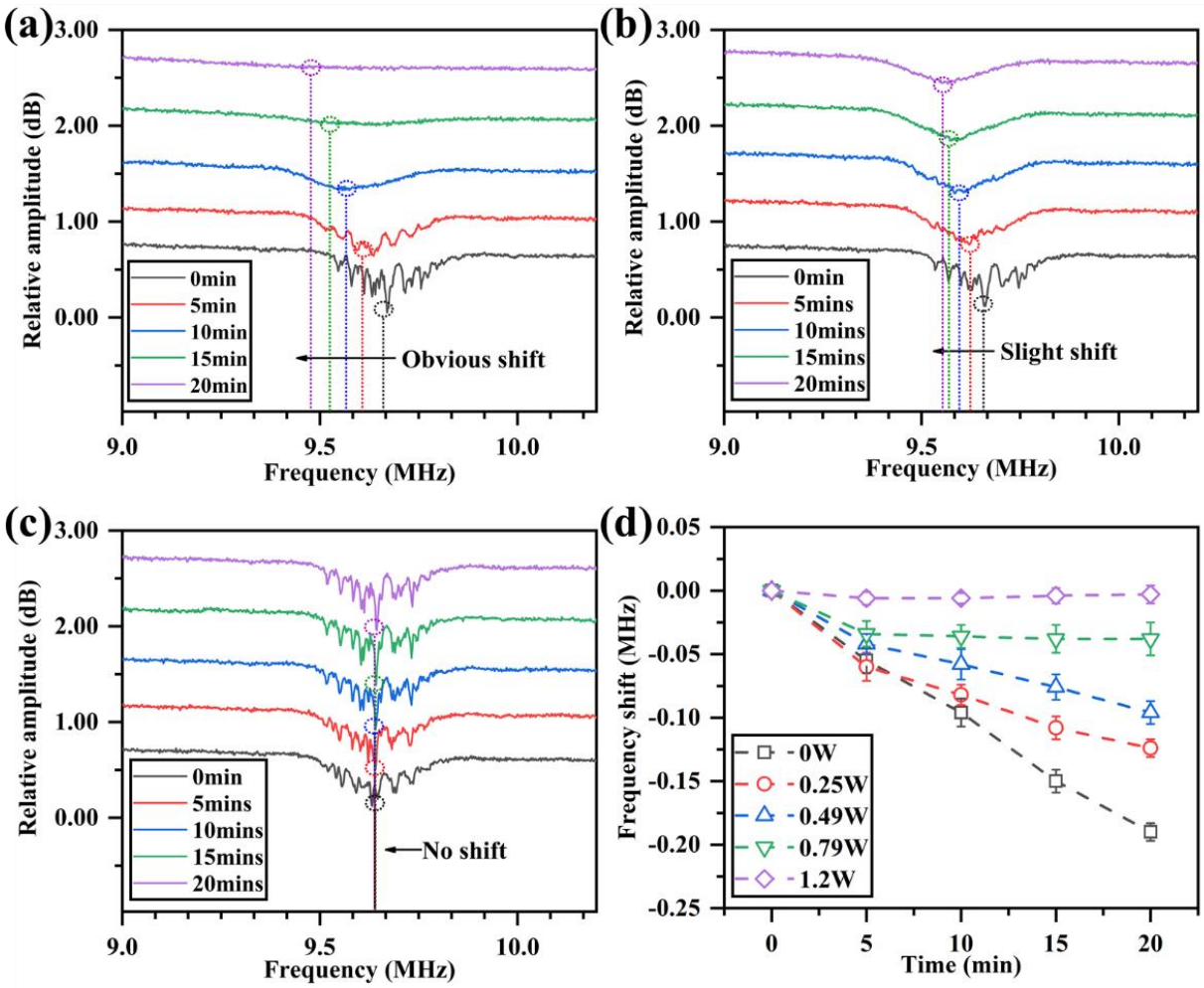

Figure 5. (a)-(c) The feedback signal of SAW with 0 W, 0.49 W, and 1.20W power applied on POTS deposited 300 μm SAW device during aerosol supplied icing process; (d) normalized resonant frequency shift of POTS deposited 300 μm SAW device with various powers during aerosol supplied icing process.

Table 1. Icing time of various samples with different wavelengths and applied powers.

Power/W	Icing time of SAW devices with various wavelengths/s			
	100μm	200μm	300μm	400μm
0	50±4			
0.07	78±5	80±4	95±7	>600
0.15	63±8	237±10	>600	>600
0.25	109±8	>600	>600	>600

A new strategy for ice prevention and removal by introducing thin film surface acoustic waves (SAWs) is presented. Highly efficient anti-icing and de-icing performance are achieved due to the combined effects from the nanoscale ‘earthquake’-like vibration, acousto-thermal heating, and acoustic streaming force. The potential of an autonomous system for ice monitoring-removal based on SAW devices is further demonstrated.

Deyu Yang, Ran Tao, Xianghui Hou*, Hamdi Torun, Glen McHale, James Martin, Yongqing Fu*

Title: Nanoscale ‘earthquake’ effect induced by thin film surface acoustic waves as a new strategy for ice protection

ToC figure